

SHUTTLE WING PANEL STABILITY ANALYSIS

T. Balderes, P. Mason, E. Ranalli,

J. Zalesak, and A. Levy

Grumman Aerospace Corporation

SUMMARY

The use of the NASTRAN program in the Shuttle wing stability analysis is described. Details of the actual structure, the finite element idealization, and the NASTRAN results are given. A comparison of the NASTRAN results with those obtained with another computer program and with hand generated results indicates good agreement. An alternate approach for solving eigenvalue problems is illustrated and shows a considerable savings in computer time. Some emphasis is placed on the relationship of the NASTRAN analysis in the design process bringing out more clearly the contribution of the results and showing the importance of the mode plots. Finally, a deficiency in the NASTRAN plate elements when used to model structures made up of intersecting plates is discussed.

INTRODUCTION

The Space Shuttle wing structure (illustrated in Figure 1) is a low aspect ratio double delta with relatively light spanwise compressive load intensity (up to 875 kN/m (5000 lbs/in.) ultimate). The external skin surfaces are required to be buckle free during vehicle operation in order to insure the integrity of the Thermal Protection System (TPS) tiles. These tiles, which are composed of silic fibers, protect the vehicle's aluminum primary structure on reentry such that the maximum temperature is limited to 176°C (350°F). The design consists of closely spaced lightweight stringers which meet the dual requirements of a low cover weight and a buckle free surface. This is fairly typical of structures that have been built around the concept of the optimum compression panel, modified for shear and lateral loading. The stringer that was selected is a roll-formed stretched aluminum and is illustrated in Figure 2. The unique shape of the stringer (eight internal corners and only two hinged free elements) permitted the use of gages as low as 0.65 mm (.022 in.) while maintaining a test crippling strength of 379 MPa (55 ksi).

Large chordwise loads (normal to the stringer) were identified when the thermal loads, resulting from temperature gradients in the primary structure due to reentry heating were calculated from a comprehensive wing-fuselage finite element analysis. These loads which are approximately 175 kN/m (1000 lbs/in.) became critical for design. Modifications to the structure were thus required to overcome the general instability problem of the stiffened cover panels subjected to large chordwise loads. These modifications included the addition of a light riblet midway between the main ribs plus stiffening of the stringer cross section with bulkheads to prevent their distortion.

This paper illustrates how the NASTRAN program significantly contributed to the efforts of the stress analysts in identifying the mode shapes and the critical parameters controlling the buckling strength of the cover panels.

SYMBOLS

| | |
|--------------------|--|
| A | enclosed area of stringer |
| D | flexural stiffness of plate = $\frac{Et^3}{12(1 - \nu^2)}$ |
| E | Young's modulus of elasticity |
| G | shear modulus |
| (GI) _{xy} | average torsional rigidity of plate |
| I | moment of inertia |
| J | torsional constant for stiffeners |
| L | length of plate, distance between main ribs |
| N | applied load intensity |
| T | work of external loads |
| T' | torque |
| V | strain energy |
| a | width of plate, distance between spars |
| b | distance between stiffeners |
| m | number of half waves in width of plate |
| t | thickness of plate |
| w | displacement normal to plate |
| λ | wavelength parameter |
| ν | Poisson's ratio |
| | Subscripts |
| cr | critical |
| p | plate |
| SB | stringer bending |
| ST | stringer torsion |

DISCUSSION

Structural Model

A typical cover panel, spanning two adjacent spars and two adjacent ribs, shown in Figure 3. One quarter of the panel (ABCD) which included seven and one half stiffeners was modeled. Conditions of simple support were imposed on the rib AB to simulate a half sine wave mode existing between ribs on the continuous cover. Simple support conditions were also imposed on spar AD. Symmetric or antisymmetric boundary conditions were assumed along the symmetry planes BC and CD. The finite element model consisted of approximately 570 nodes and 600 plate elements (QUAD2). The modified hat section was modeled as a Y section as shown in Figure 3 with BAR elements added at the base of the Y to obtain the appropriate properties. Although this model represented the basic stiffness of the section, it did not account for the local distortion which proved to be significant. Local distortion of the real stringer can drop the effective torsional stiffness GJ to 12% of the St. Venant value. Connecting the two legs of the stiffener to form a Y produces a closed cell that has a GJ of about 30% of the theoretical value of the modified hat. Note that a Y section when modeled as shown in Figure 3 is virtually distortionless due to the built in truss feature and hence the full torsional stiffness calculated by the St. Venant equations for closed cells is appropriate. This closed cell value, however, is close to an effective value of 40% that would be obtained if the waist of the modified hat is included with the upper cell. This is consistent with the insertion of "blocks" to form stiffening bulkheads in the real stringer.

Figure 4 shows a CALCOMP plot of the NASTRAN model where the cover skin has been separated from the stiffeners for clarity.

NASTRAN Analysis and Results for the Basic Structure

For the NASTRAN analysis Rigid Format 5 was used, employing the inverse power method to obtain the eigenvalues and eigenvectors.

The NASTRAN results, for the basic stiffened panel without modifications, are shown in Figures 5, 6, 7 and 8. Chordwise compressive loading (perpendicular to the stringers) was applied and two different sets of boundary conditions were considered. For the modes depicted in Figures 5 and 6, symmetric conditions were enforced along boundaries BC and CD, while for the modes shown in Figure 7 antisymmetric conditions were applied along BC and symmetric along CD. The first buckling mode (for symmetric conditions) is shown in Figure 5 where the displacements of the skin and the stringers are depicted. Also included is an end view at CD which clearly shows the number of half waves (m) and the location of node lines. Figure 6 shows the next four modes with symmetric conditions. It is noted that the first four modes are coupled; that is, they involve both bending and torsion of the stiffeners while the fifth mode is a pure bending mode since the stiffeners bend only. In a similar fashion the first five buckling modes for the antisymmetric conditions are illustrated in Figure 7. The NASTRAN results have been plotted in nondimensional form against m , the number of half waves in the

length of the panel, in Figure 8. Note that while the results for the symmetric and antisymmetric boundary conditions are very close, they do not overlap. The reason for this is that the stresses in the prebuckled state are slightly different due to the difference in the boundary conditions.

Comparison of NASTRAN Results

The NASTRAN results can be compared with results obtained with another computer program, VIPASA, which is described in Reference 1. This program treats symmetric structures consisting of long plates connected along longitudinal lines. The cover sheet and stringers were modeled with a series of 0.762-m- (30 in.) long, flat plates. The VIPASA model did not employ a Y-section representation of the stringer, as did the NASTRAN model, but followed closely the actual geometric outline accounting for chem milling patterns as shown in Figure 2. The first five VIPASA mode shapes, along with the critical loads, are shown in Figure 9 for the case of symmetric boundary conditions. The mode shapes obtained with the VIPASA program are identical to those obtained with NASTRAN; however, the order of the modes and the values of the critical loads differ.

A further comparison of the NASTRAN results involved the use of hand calculations. Two different approaches were employed. In the first, the stiffened cover panel was treated as an orthotropic plate, and in the second, the energy method was used to obtain critical loads. Figure 10 illustrates the application of orthotropic plate theory to the stiffened panel. The governing equations (see Reference 2) together with the assumed mode shape, which takes on a half sine wave along the length of the stiffeners and varies in the other direction, are shown. Note that the orthotropic plate equations in Figure 10 neglect the torsional stiffness of the stiffeners and coupling between the membrane and bending stresses due to the shift in the neutral axis. The coupling effect can be taken into account by employing a more general orthotropic plate theory as in Reference 3. However, this leads to a complicated set of equations which must be solved using a computer. Furthermore, in the calculations employed herein, v_x is taken to be zero and the stringer contribution to $(GI)_{xy}$ (the plate torsional rigidity) was neglected. Results are shown in Figure 8. Note that while the overall trend agrees with the NASTRAN results in general, lower buckling loads were obtained with the difference decreasing with m .

The use of the energy method is shown in Figure 11. Here a mode shape was assumed, and the strain energy due to plate bending, stringer bending and torsion and the potential of the applied loads was computed. Application of the principle of minimum potential energy then resulted in a value for the buckling load. Five different modes were assumed which are depicted in Figure 12 together with their respective buckling loads. Note that in this approach the interaction between the stringers and the plate is not fully accounted for. As shown in Reference 2 this interaction is a function of the mode shape. An approximate way of accounting for this effect is suggested by Timoshenko in Reference 4 and involves computing the moment of inertia of the stringers about the bottom of the plate. The torsional constant for the stiffeners was taken as 30% of the theoretical value of the modified hat section so that consistency with the finite element model is maintained. Results obtained with the energy method are also plotted in Figure 8 and show excellent agreement with the NASTRAN results.

Use of the ALARM Subprogram

The aforementioned NASTRAN analyses had between 2724 and 2853 degrees of freedom. Computer time is listed in Table 1. Also of considerable importance is the elapsed time or wall time which ranged from 5 to 10 hours for these runs. With such extensive computer residence periods, the computing system reliability becomes an important factor. In fact several computer system "crashes" were experienced during this effort which resulted in lost calendar time.

For these reasons, and in anticipation of analyses with an even greater number of degrees of freedom, an alternate approach was investigated for solving large eigenvalue problems. The concept was to use a very fast eigenvalue solution algorithm developed by Ojalvo and Newman (Reference 5) which was implemented into a working program for a NASA contract (Reference 6). This subprogram, called ALARM (Automatic Large Reduction of Matrices) employs an automatic tridiagonal reduction technique which is identical to the FEER routine described in Reference 7. The procedure was to generate the stiffness and incremental stiffness matrices in NASTRAN and then to use ALARM to obtain the desired number of eigenvalues and eigenvectors. The modes were then passed back to NASTRAN to be plotted. Table 1 shows a comparison of the eigenvalues obtained from NASTRAN and ALARM. The savings in computer time is evident from the comparison depicted in Table 3, which shows that the NASTRAN-ALARM-NASTRAN procedure reduced the computer cost by two-thirds. It should be noted that the ALARM values given in Table 2 are for the 17th iteration, and that after the first iteration the first five eigenvalues agree with those in Table 2 to four figures. Thus, the number of iterations could be cut to 2 or 3 which would result in a decrease of one-half in computer time for the ALARM step.

THE RELATIONSHIP OF THE NASTRAN ANALYSIS
TO SHUTTLE WING DESIGN CONSIDERATIONS

In the previous discussion comparisons have been made between the NASTRAN results and values obtained by using other approaches. It is advantageous to attempt to tie the various analytical and design activities together to obtain a more comprehensive view of the problem. Figure 13 illustrates the relationship of several activities that have taken place relative to the Shuttle Wing instability problem.

Initially all stability calculations were performed using hand methods (energy techniques using assumed mode shapes). Obviously these methods are limited, the results being only as good as the assumed mode shape. Attempting to guess at the lowest mode for overall instability can be difficult if not impossible (needless to say it is dangerous as well). Thus the NASTRAN analysis was undertaken to provide an overall check on the assumptions that were employed in the hand calculations. As such, the first NASTRAN analysis duplicated the design without the intermediate riblet, while the second analysis incorporated the riblet. The main purpose of the riblet is to prevent the mode that consists of alternate bending of the stringers. Having prevented this type of motion, it was discovered from the NASTRAN analysis that the stringer was still twisting as it passed over the intermediate riblet. (See Figure 14(a).) In order to prevent this, it was decided to control the clearance between the stud and the flange of the riblet (see Figure 15), such that when the stringer twisted it would come into contact with the flange of the riblet. The riblet flange was modeled as a tie bar and the results of this modification are shown in Table 4 and Figure 14(b).

Cross-sectional NASTRAN plots indicated that the stringer section was still distorting as it passed over the riblet. At this point we began to question the adequacy of the NASTRAN representation of the torsional stiffness of the stringer and in fact the effective GJ of the real stringer. To answer some of these questions a series of stiffener studies was initiated. An individual stringer and a 102 m (4 in.) width of skin was modeled as an assemblage of bars, beams, torque tubes and shear panels. This model more accurately preserved the geometric shape of the real stringer. The model was analyzed for a sine wave distribution of torque applied at the skin stringer attachment and for a concentrated torque applied at the end of the .381m (15 in.) length. Results of this latter analysis were correlated with test data. A cross-sectional plot of the model and the deformed shape at different stringer stations is shown in Figure 16. Note the severe bending distortion of the cross section at the loaded end and that the distortion decreases with the stringer station. If the stringer were long enough, the distortion would completely disappear, an indication that the total torque would then be taken by St. Venant torsion. The sine wave torque loading (comparable to the distribution of torsion that the stringer would have to resist to prevent buckling) was used to calculate an effective GJ value for the stringer. The calculated value was approximately 12% of the St. Venant torsional stiffness. At this point several design changes were considered. These included adding "blocks" at various spacings which tied the two sides of the stringer together at the waist (see Figure 17(a)). This scheme tends to mobilize the upper portion

of the stringer. A second concept was to insert a vertical "spike" through the stringer to tie the cover to the bottom and two sides of the stringer (see Figure 17(b)). This scheme is far more effective than the block scheme but also weighs more. A third possibility was also initiated, which was to investigate an alternate stringer concept that would not be subject to large distortion under torsional loading.

The Shuttle Wing design 101 used a combination of blocks and spikes. A spike was placed adjacent to each of the riblet attachment points. This configuration was investigated by modifying the previous NASTRAN model. The results of the analysis are shown in Table 4. The final NASTRAN analysis consisted of adding a beam element to the skin parallel to the intermediate riblet. This last modification which prevented bending of the skin along the riblet did little to increase the buckling allowable.

Some concern was developed at this time over the adequacy of elements in NASTRAN to predict the buckling behavior of structures composed of QUAD2 plate elements that intersect at an angle. In the QUAD2 elements, the inplane motion is assumed to be linear between node points while the out of plane motion is essentially a cubic. An incompatibility problem thus inherently exists such that elements connected at angles to each other do not continuously reinforce one another, but instead are "stitched" together at the nodes. In addition to this, the elements lack torsional stiffeners normal to their plane. Thus, as a separate study, the QUAD2 elements were used to obtain the buckling modes of an equal leg angle column. It was discovered that while the torsional buckling mode of the angle could be obtained using a refined grid, convergence was from the low side. Furthermore, some peculiar modes were observed and the Euler buckling mode could not be obtained. In order to clarify this problem, an investigation to determine the applicability of higher order plate elements (as described in Reference 8) has been initiated. These concerns caused us to turn to an alternate analytical approach, the VIPASA program. VIPASA can model continuous structure in detail. It cannot, however, account for discrete stiffening or items that do not fit into a Fourier series expansion. The correlation of the VIPASA results has been discussed previously.

As discussed above, work was initiated to develop an alternate stringer concept with the prime goal of minimizing the local distortion. This involved the analysis of a typical unit width of stringer with a torsion load applied at the skin line which is balanced with a $\left(\frac{T}{2A}\right)$ shear flow distribution. The stringer behaves as a frame, and hence has an internal force and moment distribution. Dividing the moment by the force gives the location of the load line. The geometric shape of the stringer was then modified to straddle the load line, keeping in mind other considerations such as local crippling requirements, fabrication restrictions and clearances dictated by the present design. The process of analysis and geometric modification was iterated until a stringer of the shape shown in Figure 17(c) was obtained. The effective GJ of this stringer is approximately 5 times the effective GJ of the unreinforced modified hat. Work is not yet complete on this concept but strong consideration is being given to it for inclusion in future Shuttle Wing designs.

A useful plot that illustrates the effects of the various design parameters is shown in Figure 18 where the critical stress is plotted as a function of the

unsupported stringer length. The plot was obtained using the energy equations given in Figure 11. The plot illustrates the improvement in allowable buckling stress in using the frame stiffened hat over the modified hat. Buckling stresses are indicated for a range of modified hat effective GJ values; the particular value within the range depends on the combination of block and spike spacing and stringer length. Note that the effective GJ for a stringer varies with length and is equal to the St. Venant value at $L = \infty$ and virtually zero for $L = 0$. It also should be noted that from a practical point of view one can question the real effectiveness of the blocks and spikes as these quantities are related to various manufacturing procedures. The four lowest NASTRAN values from Table 4 have been superimposed on the plot at spacings of 0.762m (30 in.) and 0.381m (15 in.). NASTRAN analysis I did not include the riblet; analysis II did but did not prevent twisting at the riblet support (hence it is lower than the value predicted by the hand calculations which tacitly assume zero rotation at the supports). NASTRAN analysis III prevented rotation at the support but not distortion. Analysis IV prevented rotation and distortion by inserting a spike at the riblet.

The plot also indicates the improvement in buckling stress due to inserting the riblet (spacing changes from 0.762m (30 in.) to 0.381m (15 in.)) which prevents the first bending mode.

It is important to note that simplified tests of the stiffened panel, under transverse compressive loading, correlated well with some but not all of the analytical results. In general, the large strength increases in the bending and coupled modes due to the addition of the riblet were attained. Also, the improvement in the effective torsional stiffness of the stringer with the block and spike modifications was corroborated. For the torsion modes, however, an effective length reduction from 0.762m (30 in.) to 0.381m (15 in.) proved difficult to attain. Subsequent analysis, using hand computations, showed that these lower than expected strength levels could be traced to the low torsional stiffness provided at mid bay. In effect the torsional restraint at the riblet was too flexible and allowed twisting as the plate buckled. This agreed with test observations. These results demonstrate the need to provide and model accurately the local stiffness which affect the behavior of the actual structure.

CONCLUDING REMARKS

The use of the NASTRAN program in the stability analysis of the Shuttle wing panels has been described. Moreover, the role of the NASTRAN analysis in the design process has been discussed to illustrate how it impacted the design. The NASTRAN results helped to identify the critical modes and show the importance of the torsional properties of the stiffeners. In this effort, the NASTRAN plots of the mode shapes were indispensable in that they indicated where the fixes should be made and clearly demonstrated their effectiveness. The results indicated that for future analyses (which will include spanwise loading in addition to the chordwise loading to determine the interaction effects) a better representation of the stringers is required.

It was demonstrated that a tridiagonal reduction scheme can greatly reduce the computer cost in solving large eigenvalue problems.

Finally, it was discovered that the plate bending elements in NASTRAN have incompatibilities which can lead to difficulties when the elements are used to model structures made up of intersecting plates. Further work in this area is clearly required to develop a plate bending element which would overcome the present deficiencies.

ACKNOWLEDGEMENTS

Acknowledgement is extended to the many contributors in the effort presented herein. Many of the design concepts were defined by I.G. Hedrick, L. Mead, T. Adee, D. Bone and J. Strakosch; specifically, the development of the frame stiffened hat concept is due to L. B. Wehle. The analysis using the VIPASA program was performed by M. Anderson of NASA Langley. A considerable part of the hand calculations was done by G. Kutz and L. Brown.

REFERENCES

1. Wittrick, W. H., and Williams, F. W., "Buckling and Vibration of Anisotropic or Isotropic Assemblies Under Combined Loadings," Int. J. Mech. Sci., Pergamon Press, 1974, Vol. 16, pp.209-239.
2. Seide, P., "The Effect of Longitudinal Stiffeners Located on One Side of a Plate or the Compressive Buckling Stress of the Plate Stiffening Combination," NACA TN 2873, Jan. 1953.
3. Ashton, J. E., Halpin, J. C., Petit, P. H., "Primer on Composite Materials: Analysis," Technomic Publishing Co., Stamford, CT, 1969.
4. Timoshenko, S. P., and Gere, J. M., "Theory of Elastic Stability," McGraw-Hill Book Co., 1961.
5. Ojalvo, I.U., and Newman, M., "Vibration of Large Structures by an Automatic Matrix Reduction Method," AIAA Journal, Vol. 8, No. 7, 1970, pp.1234-1239.
6. Ojalvo, I. U., Austin, F., and Levy, A., "Vibration and Stress Analysis of Soft-Bonded Shuttle Insulation Tiles," NASA CR-132553, Sept. 1974.
7. Newman, M., and Pipano, A., "Fast Modal Extraction in NASTRAN via the FEER Computer Program," Third NASTRAN User's Colloquium, NASA TM X-2893, Sept.1973.
8. Pifko, A., Levine, H. S., and Armen, H., Jr., "PLANS--A Finite Element Program for Nonlinear Analysis of Structures - Vol. I - Theoretical Manual," Grumman Aerospace Research Dept., Report RE-501, August 1974.

TABLE 1 - NASTRAN BUCKLING ANALYSIS

| MODE SET | NUMBER OF MODES | NO. OF D.O.F. | CPU MIN |
|----------|-----------------|---------------|---------|
| 1 | 11 | 2837 | 68.90 |
| 2 | 10 | 2853 | 81.16 |
| 3 | 10 | 2724 | 81.46 |
| 4 | 10 | 2724 | 73.51 |
| 5 | 10 | 2724 | 95.40 |
| 6 | 4 | 2724 | 38.00 |

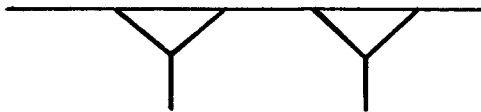
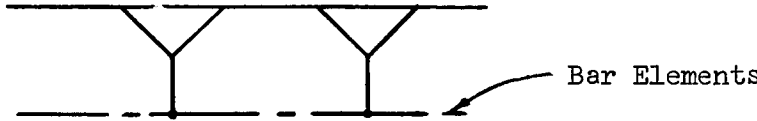
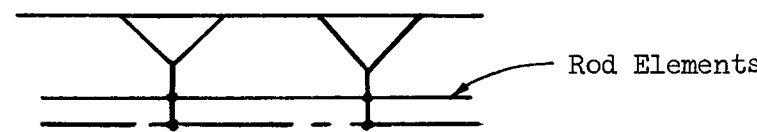
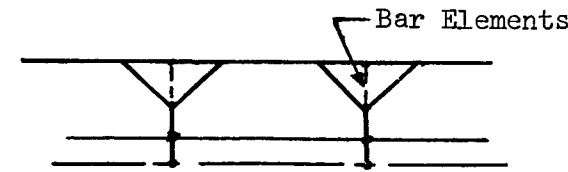
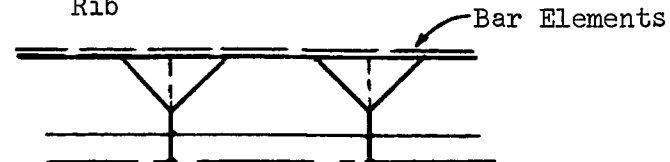
TABLE 2 - RESULTS FOR MODE SET 3

| MODE | EIGENVALUE | |
|------|------------|----------|
| | NASTRAN | ALARM |
| 1 | .8352054 | .8352112 |
| 2 | .9625223 | .9625288 |
| 3 | 1.147742 | 1.147748 |
| 4 | 1.363301 | 1.363310 |
| 5 | 1.592074 | 1.592082 |
| 6 | 1.828479 | 1.828488 |
| 7 | 2.053671 | 2.050866 |
| 8 | 2.057876 | 2.069090 |
| 9 | 2.058429 | 2.217536 |
| 10 | 2.060794 | 2.327002 |

TABLE 3 - NASTRAN-ALARM COMPARISON

| | NASTRAN | | ALARM | |
|------------------------|---------|-----------|-------|-----------|
| | CPU | WALL TIME | CPU | WALL TIME |
| 1) LINEAR ANALYSIS | 9 | 72 | 9 | 72 |
| 2) EIGENVALUE | 70 | 207 | 19 | 57 |
| 3) PLOTTING & RECOVERY | 2 | 6 | 2 | 6 |
| TOTAL | 81 | 285 | 30 | 135 |
| SYSTEM MIN. | 621.55 | | 224 | |

TABLE 4 - SUMMARY OF NASTRAN ANALYSES

| CASE | N_{cr} , kN/m (lb/in.) | | |
|---|--------------------------|-------------------------|-------------------------|
| | Mode 1 | Mode 2 | Mode 3 |
| <p>I. Basic Structure</p>  | <p>99.2 (566)</p> | <p>100.5 (574)</p> | <p>109.2 (623)</p> |
| <p>II. Intermediate Rib Added with Vertical and Rotation Supports at Rib Tie</p>  | <p>146.2 (835)</p> | <p>166.7 (952)</p> | <p>201.2 (1149)</p> |
| <p>III. Tie Bar Added at Top of Intermediate Rib</p>  | <p>215.2 (1229)</p> | <p>240.8 (1375)</p> | <p>271.3 (1549)</p> |
| <p>IV. Spike Added</p>  | <p>241.8 (1381)</p> | <p>264.3 (1509)</p> | <p>291.2 (1663)</p> |
| <p>V. Beam Added to Skin Parallel to Intermediate Rib</p>  | <p>242.7 (1386)</p> | <p>257.9 (1473)</p> | <p>280.2 (1600)</p> |

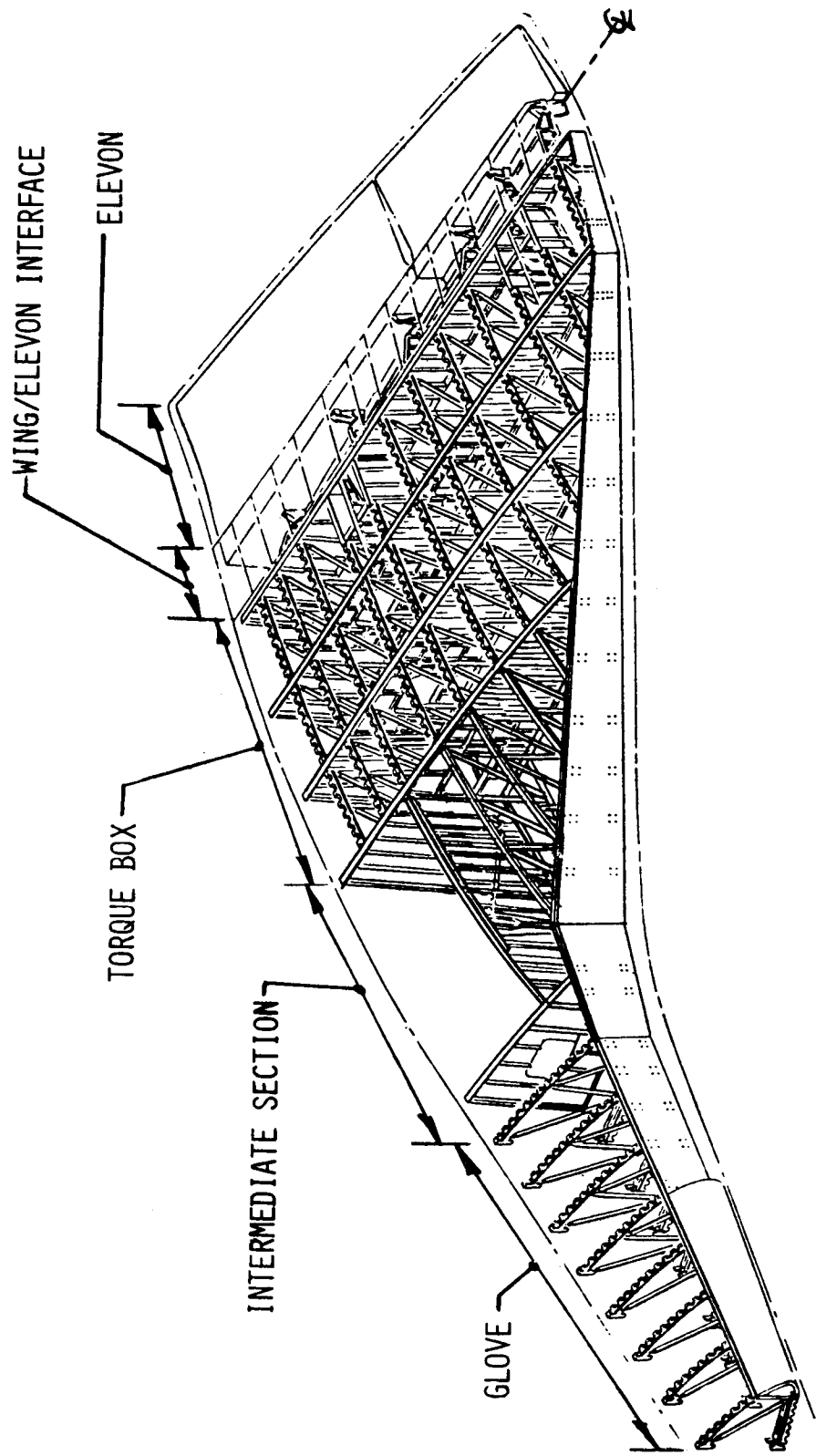


Figure 1.- Shuttle wing structure.

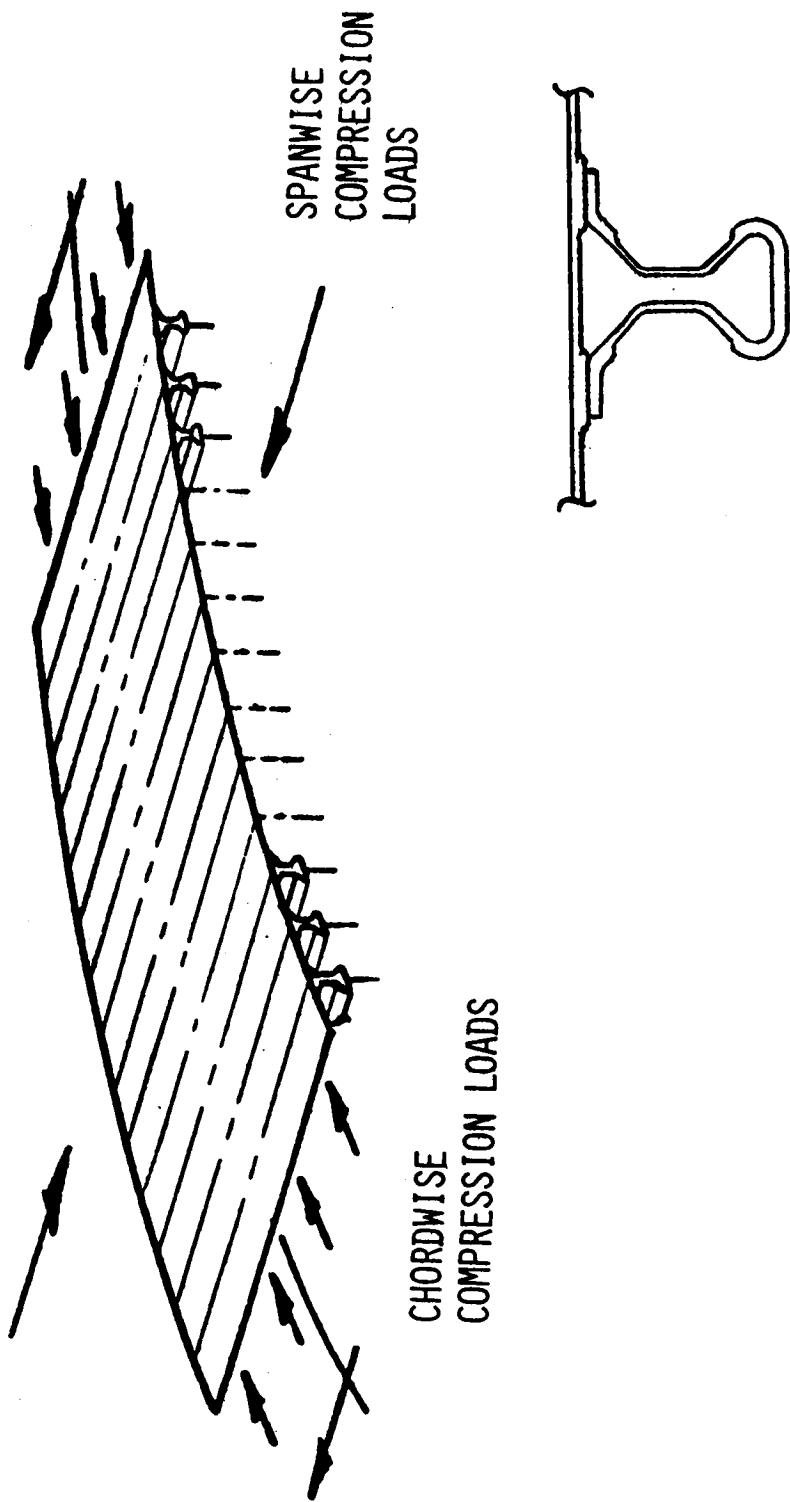


Figure 2.- Shuttle wing cover panel.

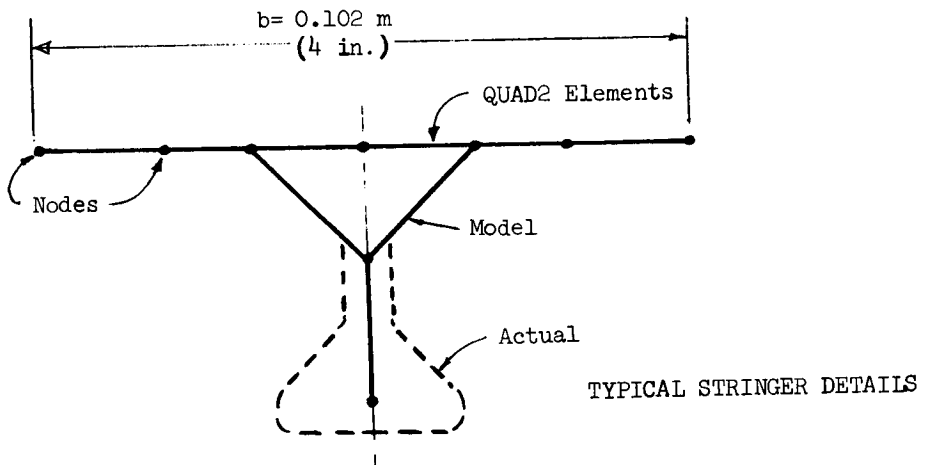
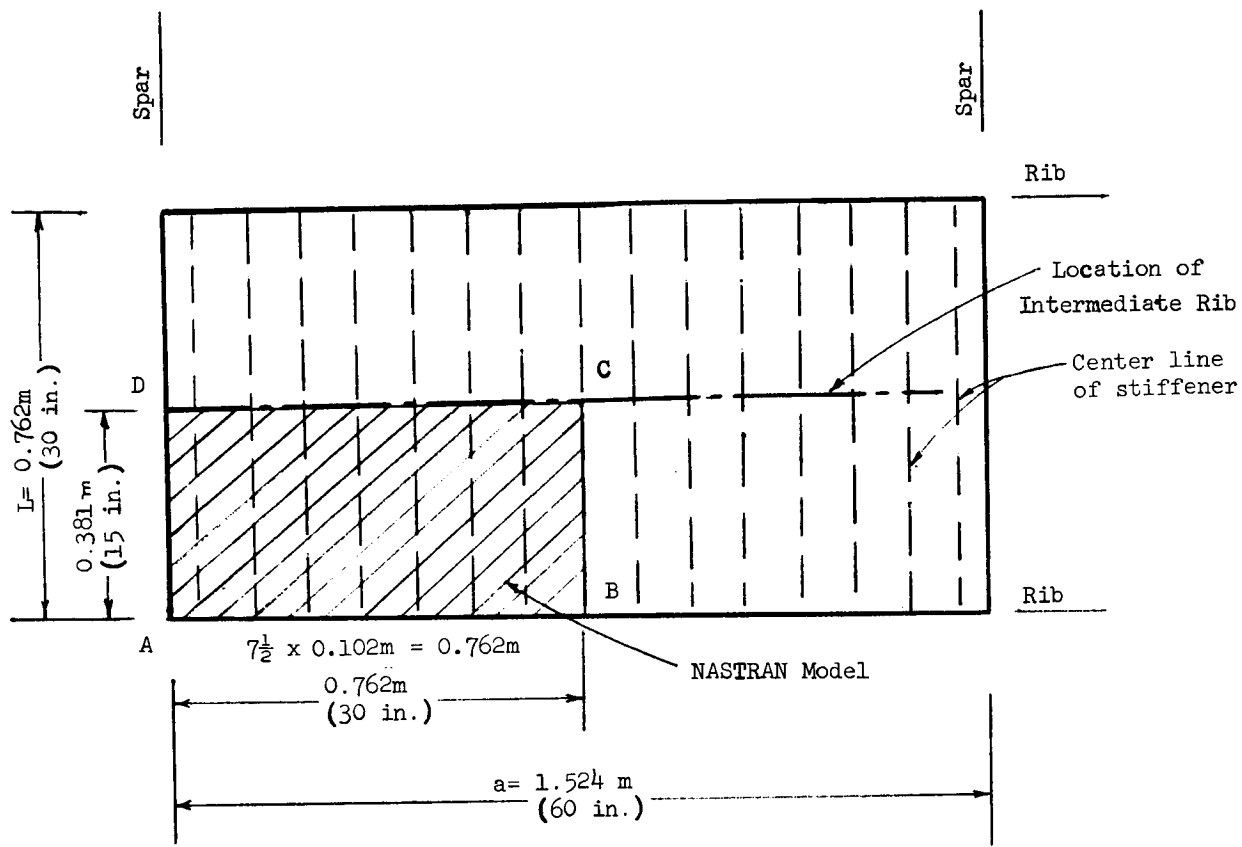
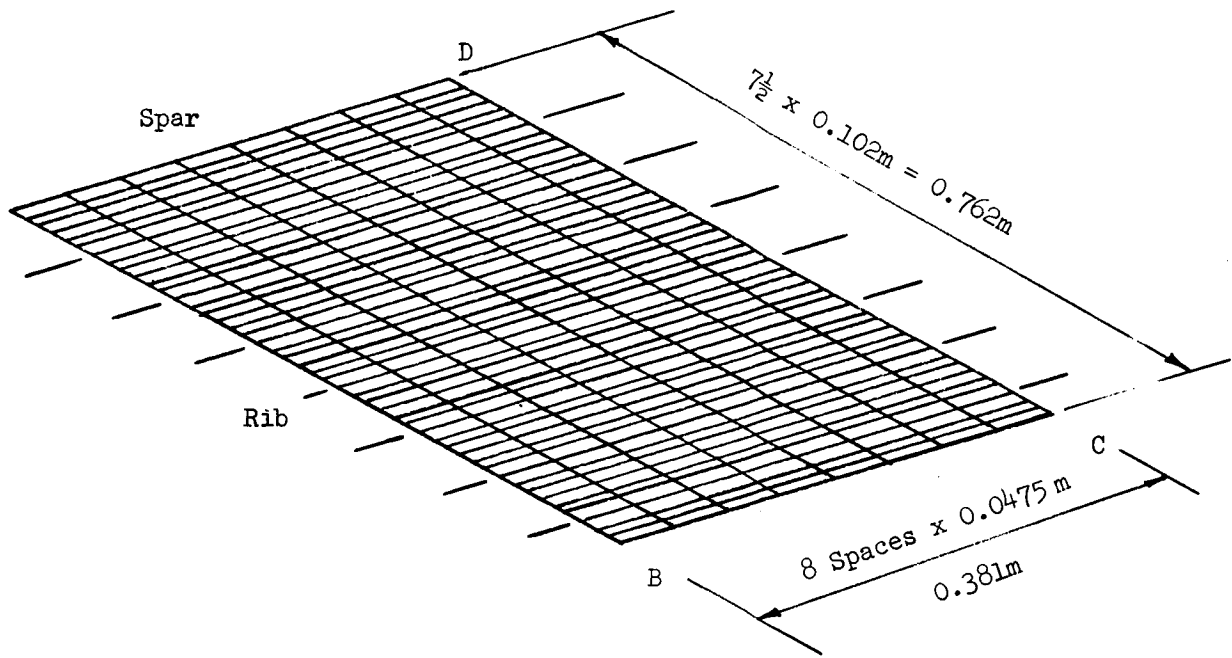
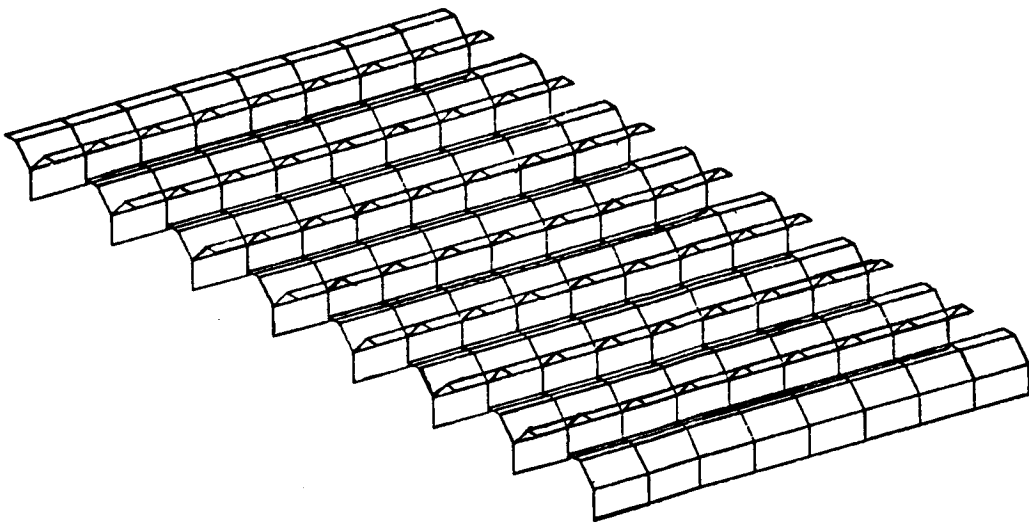


Figure 3.- Shuttle wing panel model.

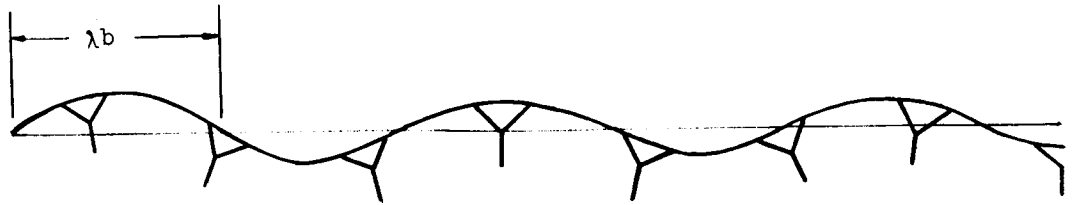


Cover Sheet



Stiffeners

Figure 4.- Plot of NASTRAN model.



$\lambda = 1.363$, $N_{cr} = 99.17 \text{ kN/m}$ (566 lb/in.) $m=11$

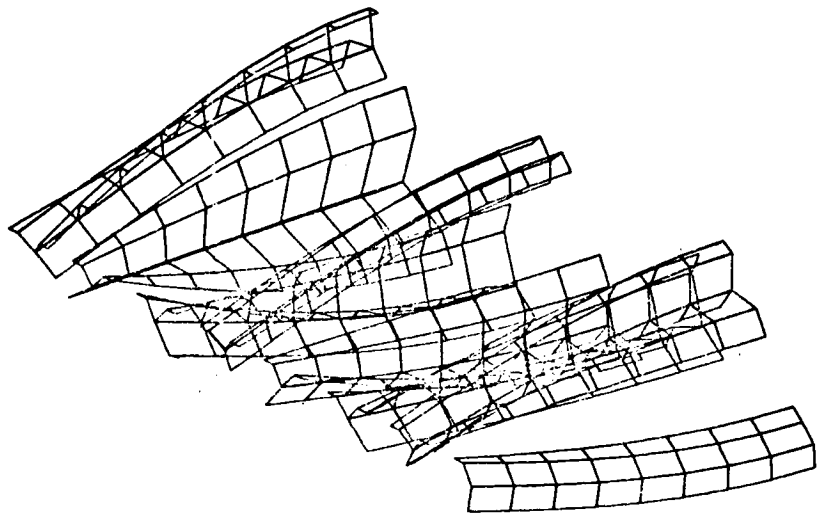
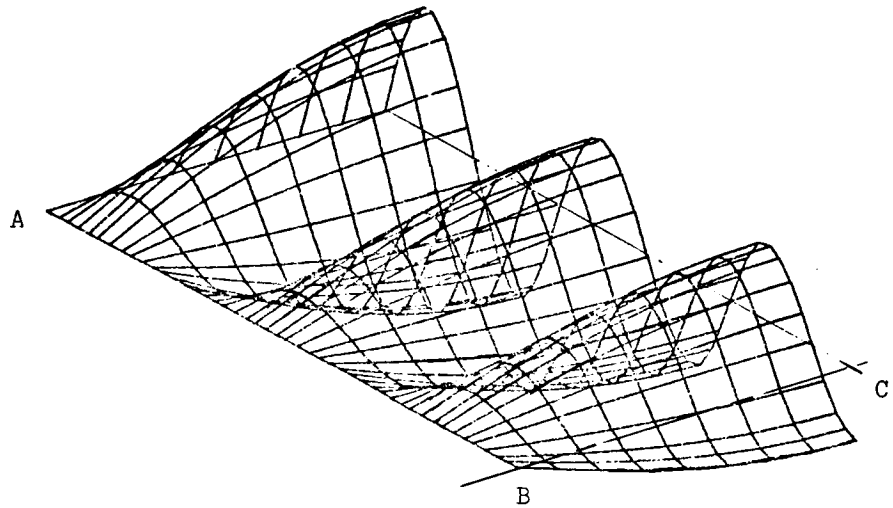
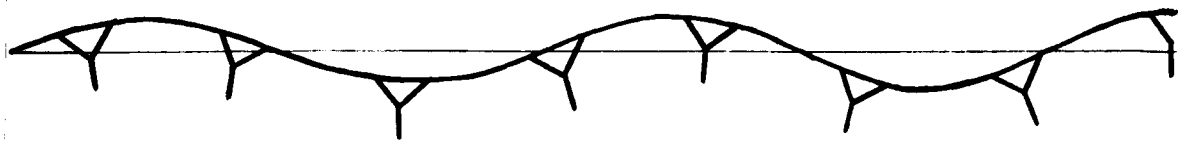


Figure 5.- NASTRAN results - mode 1 - symmetric conditions.



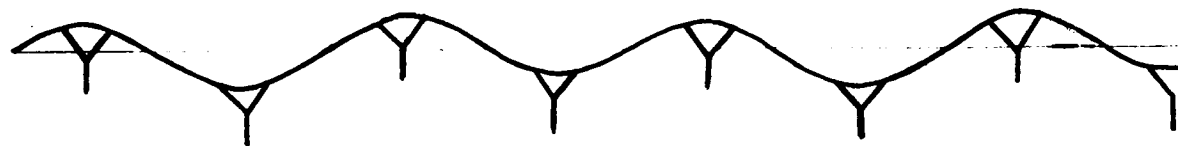
Mode 2- $\lambda = 1.666$, $N_{cr} = 100.5 \text{ kN/m (574 lb/in.)}$ $m=9$



Mode 3 - $\lambda = 1.154$, $N_{cr} = 109.2 \text{ kN/m (623 lb/in.)}$ $m=13$

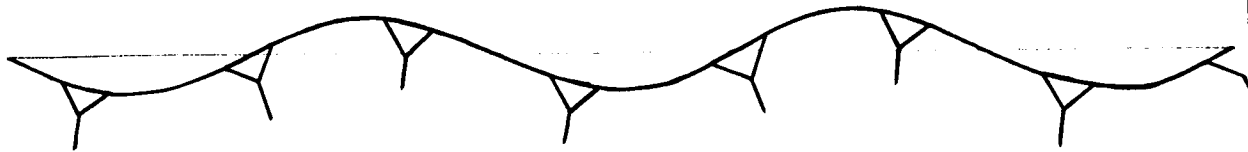


Mode 4 - $\lambda = 2.142$, $N_{cr} = 120.4 \text{ kN/m (688 lb/in.)}$ $m=7$

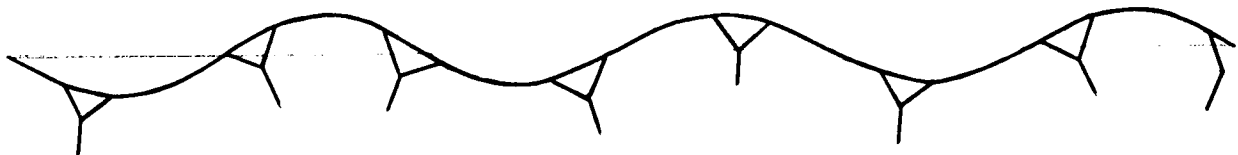


Mode 5 - $\lambda = 1.0$, $N_{cr} = 129.0 \text{ kN/m (737 lb/in.)}$ $m=15$

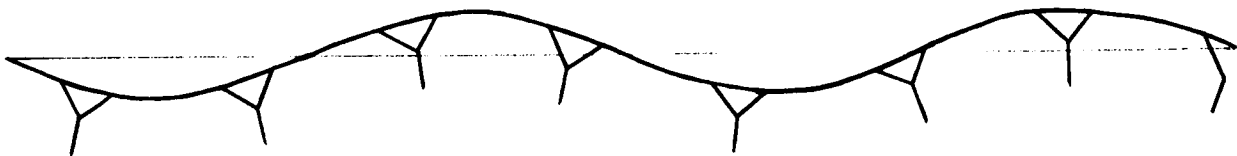
Figure 6.- NASTRAN results - modes 2-5 - symmetric conditions.



Mode 1 - $\lambda = 1.5$, $N_{cr} = 96.5 \text{ kN/m (551 lb/in)}$ $m=10$



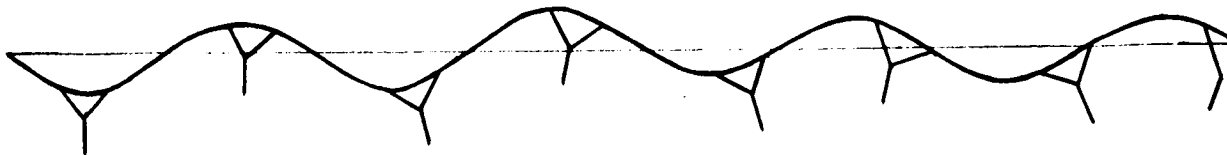
Mode 2 - $\lambda = 1.2666$, $N_{cr} = 101.6 \text{ kN/m (580 lb/in)}$ $m=12$



Mode 3 - $\lambda = 1.875$, $N_{cr} = 105.1 \text{ kN/m (600 lb/in)}$ $m=8$



Mode 4 - $\lambda = 1.071$, $N_{cr} = 114.5 \text{ kN/m (654 lb/in)}$ $m=14$



Mode 5 - $\lambda = 0.9375$, $N_{cr} = 134.9 \text{ kN/m (770 lb/in)}$ $m=16$

Figure 7.- NASTRAN results - modes 1-5 - antisymmetric conditions.

- ✱ NASTRAN - symmetric
- NASTRAN - antisymmetric
- ◇ VIPASA
- Orthotropic Plate Theory
- △ Energy Method

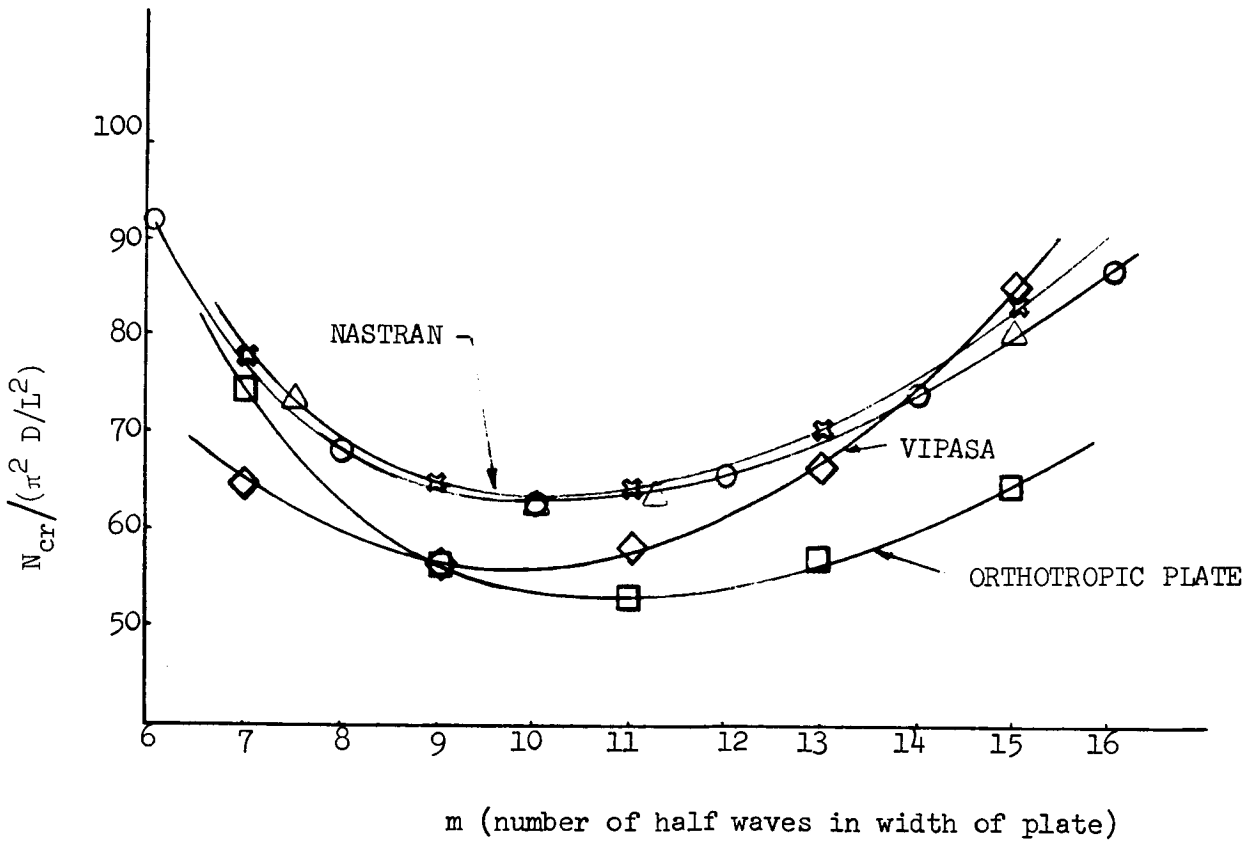
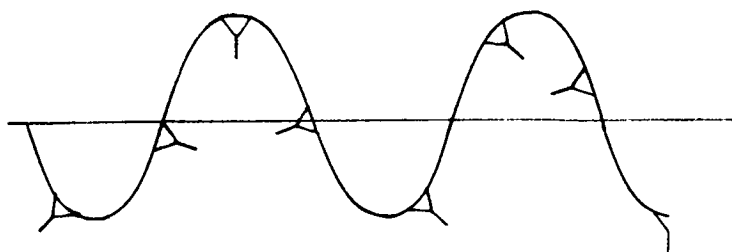


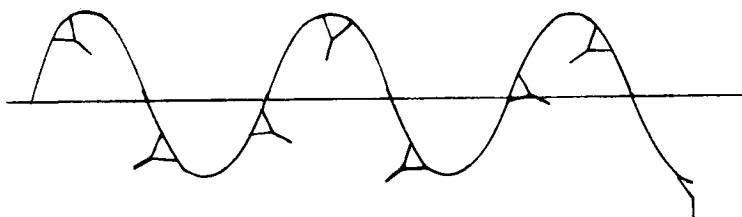
Figure 8.- Comparison of results.



$$N_{cr} = 86.8 \text{ kN/m (496 lb/in.)}$$

$$\lambda = 1.666$$

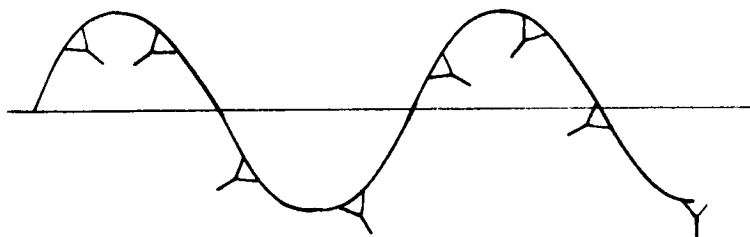
$$m = 9$$



$$N_{cr} = 90.2 \text{ kN/m (515 lb/in.)}$$

$$\lambda = 1.30$$

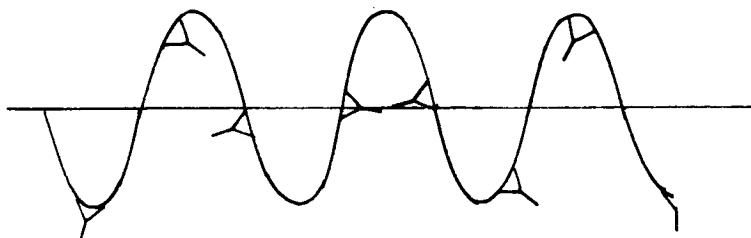
$$m = 11$$



$$N_{cr} = 99.6 \text{ kN/m (569 lb/in.)}$$

$$\lambda = 2.142$$

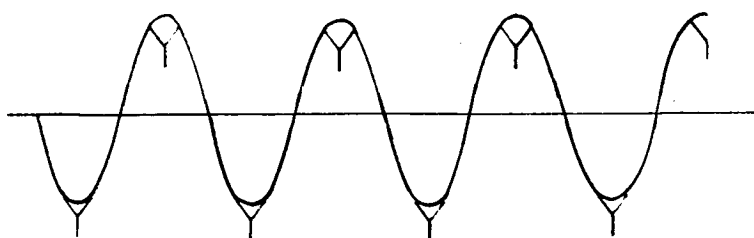
$$m = 7$$



$$N_{cr} = 101.9 \text{ kN/m (582 lb/in.)}$$

$$\lambda = 1.154$$

$$m = 13$$

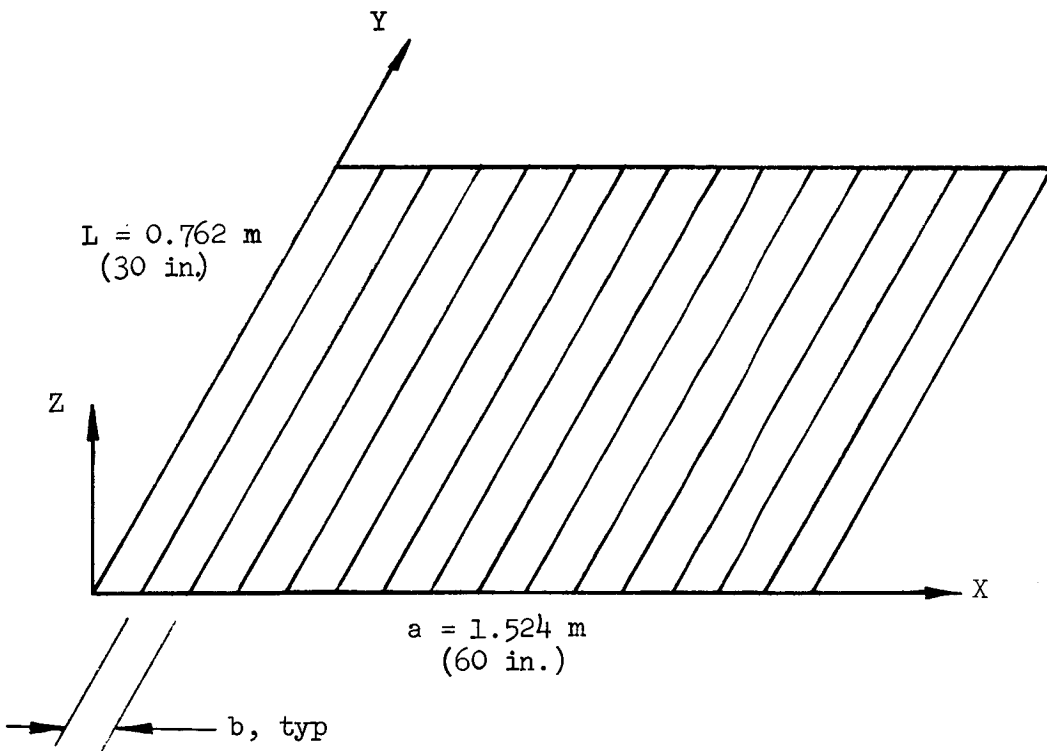


$$N_{cr} = 132.4 \text{ kN/m (756 lb/in.)}$$

$$\lambda = 1$$

$$m = 15$$

Figure 9.- Results obtained with VIPASA program.

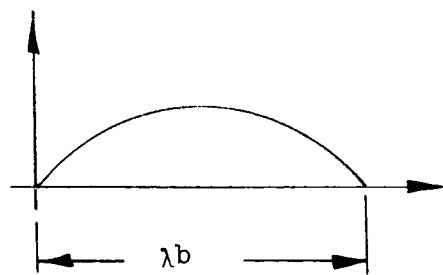


$$D_1 \frac{\partial^4 w}{\partial x^4} + 2D_3 \frac{\partial^4 w}{\partial x^2 \partial y^2} + D_2 \frac{\partial^4 w}{\partial y^4} + N_x \frac{\partial^2 w}{\partial x^2} = 0$$

where $D_1 = (EI)_x / (1 - \nu_x \nu_y)$
 $D_2 = (EI)_y / (1 - \nu_x \nu_y)$
 $D_3 = \frac{1}{2} (\nu_x D_2 + \nu_y D_1) + 2(GI)_{xy}$
 $N_x = \text{compressive load}$

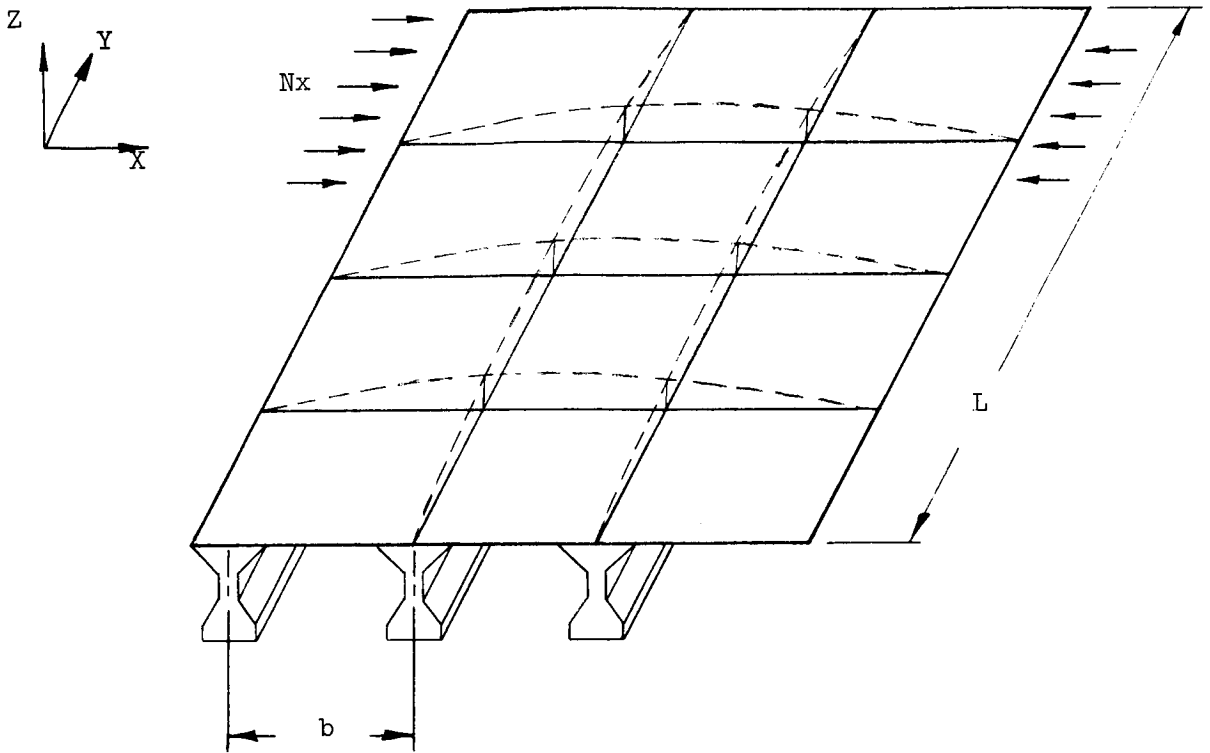
assumed mode shape

$$w = w_0 \sin \frac{\pi x}{\lambda b} \sin \frac{\pi y}{L}$$



$$N_x = D_1 \left(\frac{\pi}{\lambda b} \right)^2 + 2D_3 \left(\frac{\pi}{L} \right)^2 + D_2 \left(\frac{\pi}{L} \right)^2 \left(\frac{\lambda b}{L} \right)^2$$

Figure 10.- Orthotropic plate equations.



Assumed Mode Shape: $w = w_0 \sin \frac{\pi x}{\lambda b} \sin \frac{\pi y}{L}$

$$\Delta T = \Delta V_p + \Delta V_{SB} + \Delta V_{ST}$$

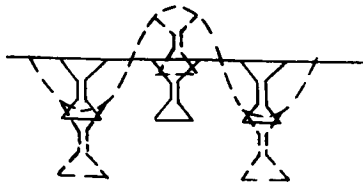
$$\Delta T = -\frac{1}{2} \iint \left[N_x \left(\frac{\partial w}{\partial x} \right)^2 + N_y \left(\frac{\partial w}{\partial y} \right)^2 + 2N_{xy} \frac{\partial w}{\partial x} \frac{\partial w}{\partial y} \right] dx dy$$

$$\Delta V_p = \frac{1}{2} D \iint \left[\left(\frac{\partial^2 w}{\partial x^2} \right)^2 + \left(\frac{\partial^2 w}{\partial y^2} \right)^2 + 2\nu \frac{\partial^2 w}{\partial x^2} \frac{\partial^2 w}{\partial y^2} + 2(1-\nu) \left(\frac{\partial^2 w}{\partial x \partial y} \right)^2 \right] dx dy$$

$$\Delta V_{SB} = \frac{EI}{2} \int \left(\frac{\partial^2 w}{\partial y^2} \right)^2 dy$$

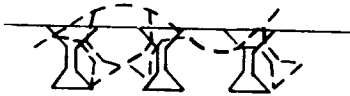
$$\Delta V_{ST} = \frac{GJ}{2} \int \left(\frac{\partial \phi}{\partial y} \right)^2 dy \quad \phi = \frac{\partial w}{\partial x}$$

Figure 11.- Energy approach.



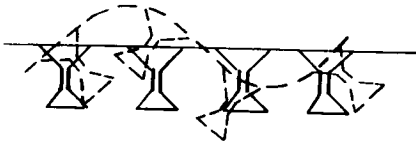
Stringer
Bending
 $\lambda = 1$
 $m = 15$

$N_{cr} = 129.9 \text{ kN/m}$
(742 lb/in.)



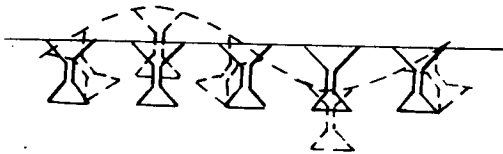
Stringer
Torsion
 $\lambda = 1$
 $m = 15$

$N_{cr} = 120.4 \text{ kN/m}$
(687 lb/in.)



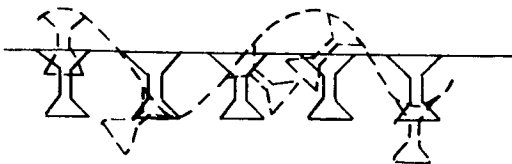
$\lambda = 1.5$
 $m = 10$

$N_{cr} = 100.9 \text{ kN/m}$
(576 lb/in.)



$\lambda = 2$
 $m = 7.5$

$N_{cr} = 118.2 \text{ kN/m}$
(675 lb/in.)



$\lambda = 1.333$
 $m = 11.25$

$N_{cr} = 101.9 \text{ kN/m}$
(582 lb/in.)

Figure 12.- Results of energy approach.

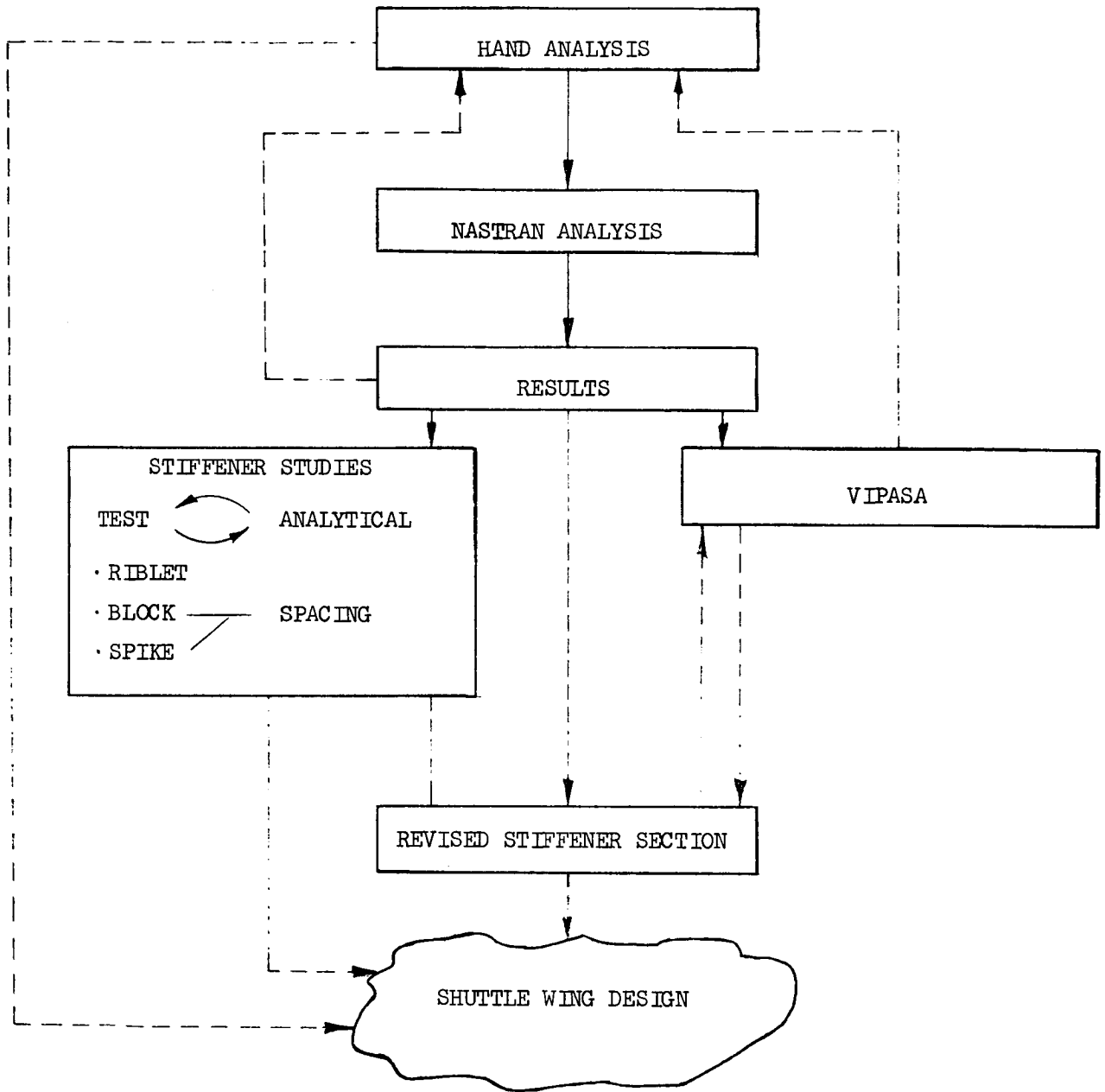
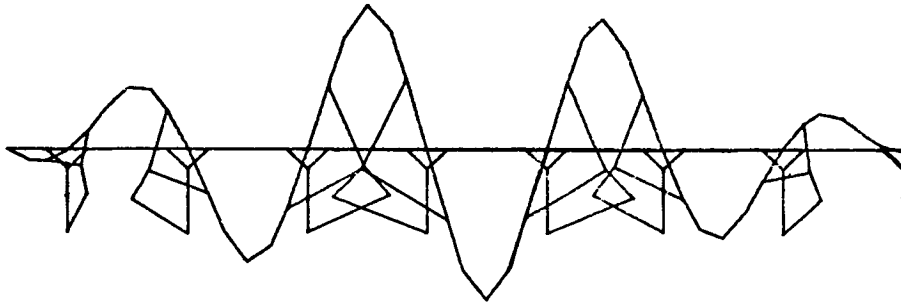


Figure 13.- Relationship of design analysis activities.



NASTRAN ANALYSIS - CASE II 1st MODE

$$N_{cr} = 146.2 \text{ kN/m (835 lb/in)}$$

(A)



NASTRAN ANALYSIS - CASE III 1st MODE

$$N_{cr} = 215.2 \text{ kN/m (1229 lb/in)}$$

(B)

Figure 14.- NASTRAN results for modified structure.

GENERAL INSTABILITY MODIFICATIONS - TYPICAL STIFFENER INSTALLATION

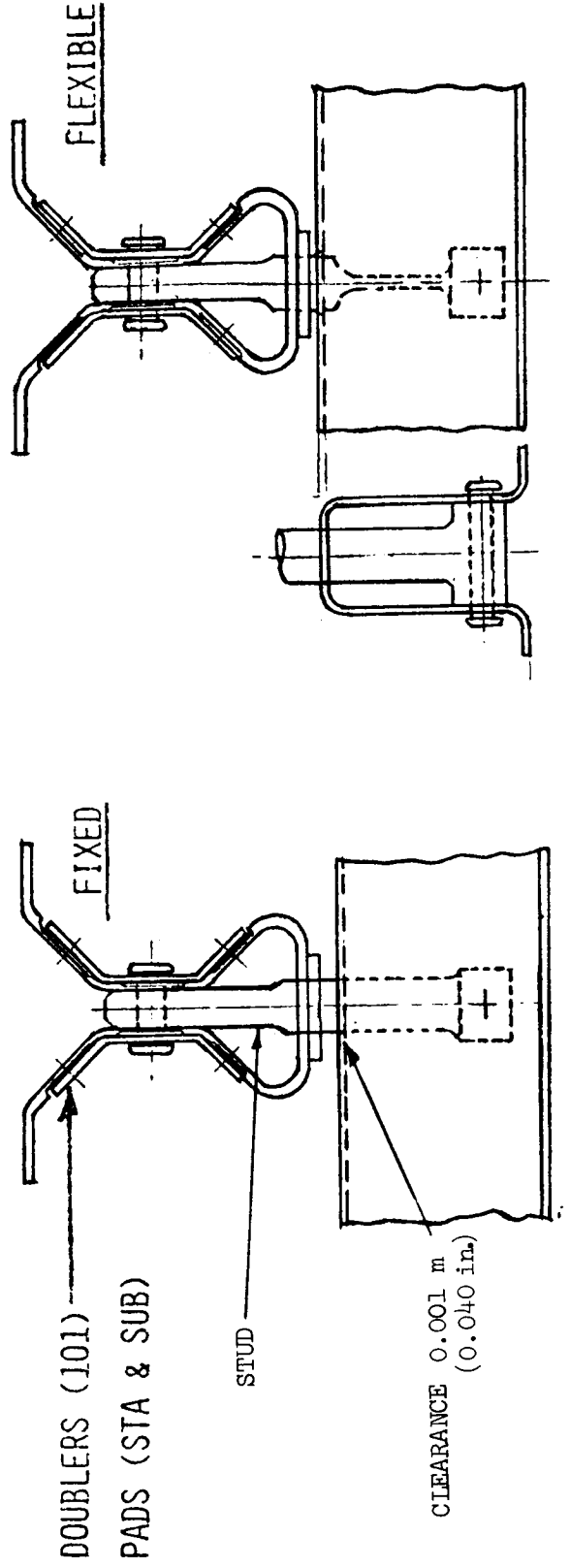
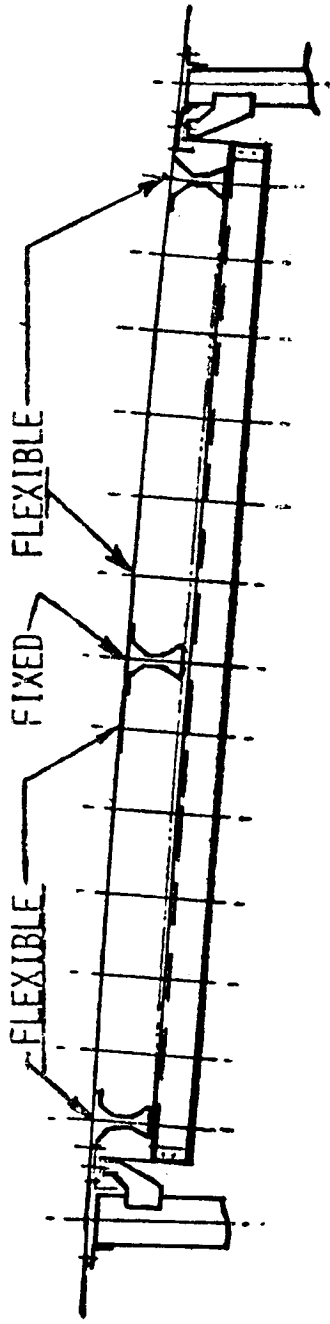


Figure 15.- Intermediate rib details.

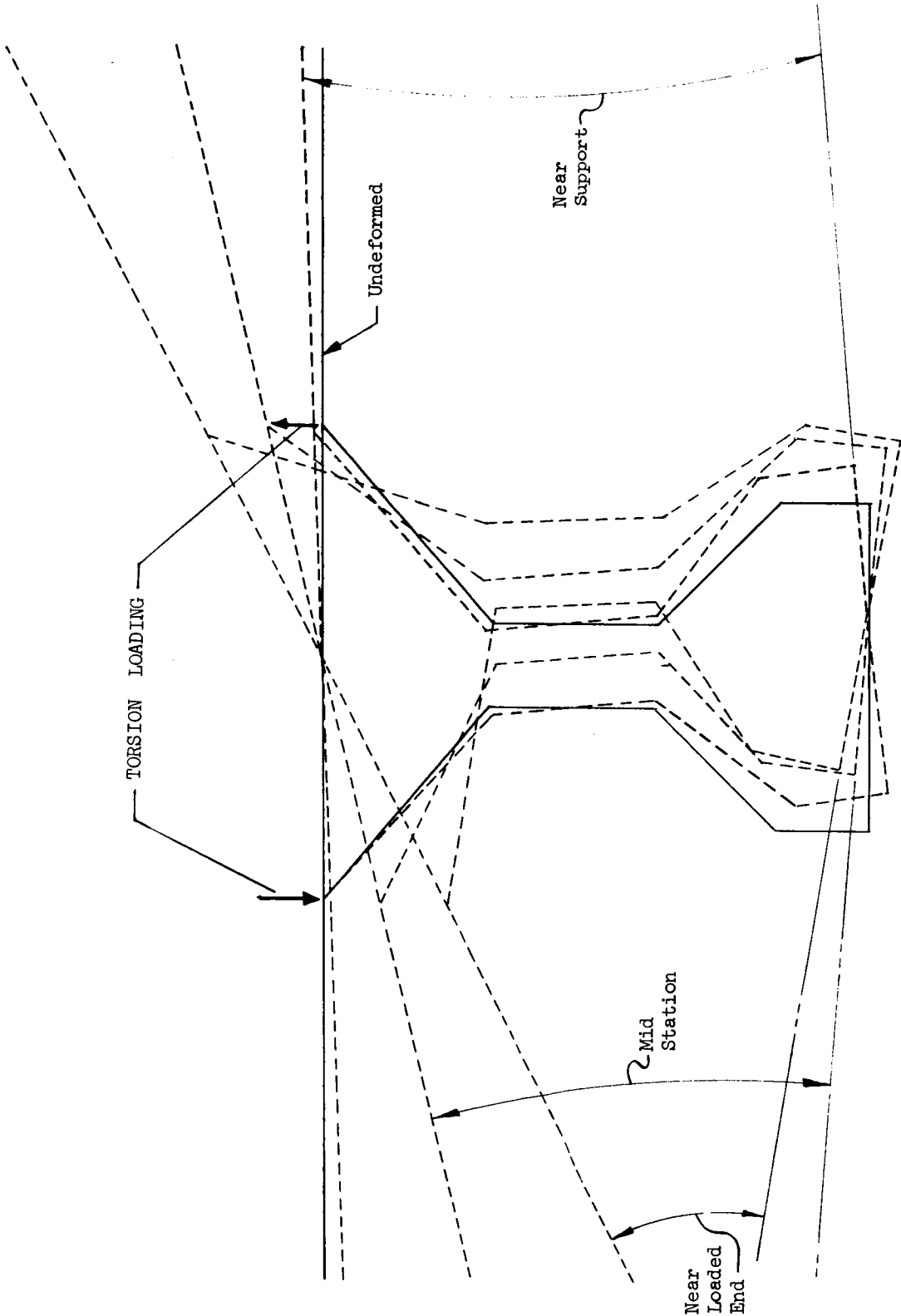
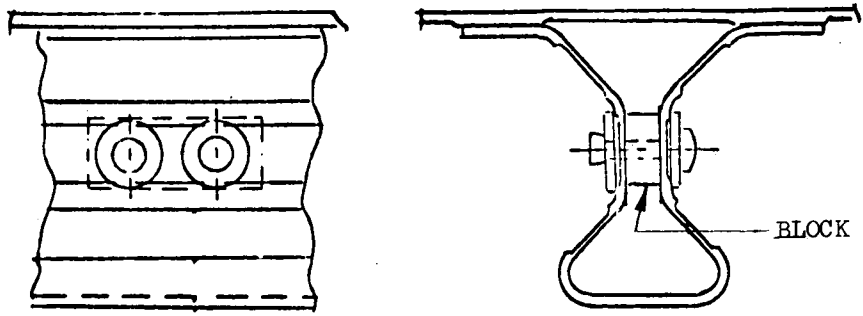
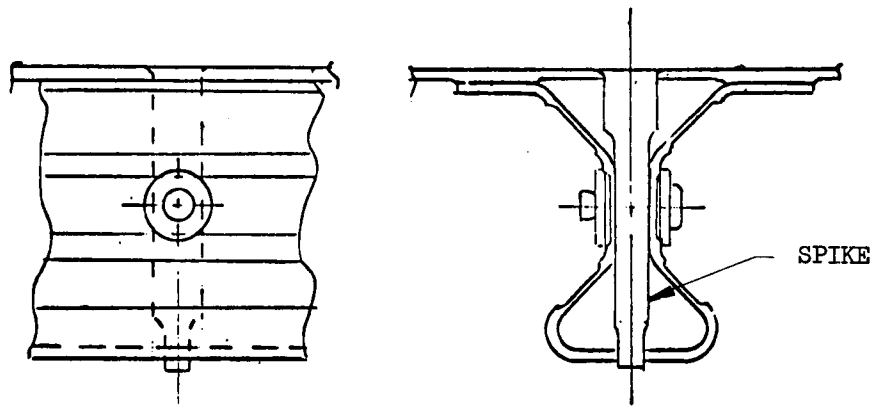


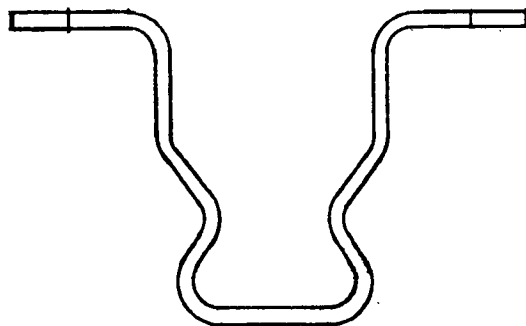
Figure 16.- Distortion of stringer.



(A) BLOCK STIFFENING



(B) SPIKE STIFFENING



(C) FRAME STIFFENED HAT
(chem milling patterns not shown)

Figure 17.- Stringer design concepts.

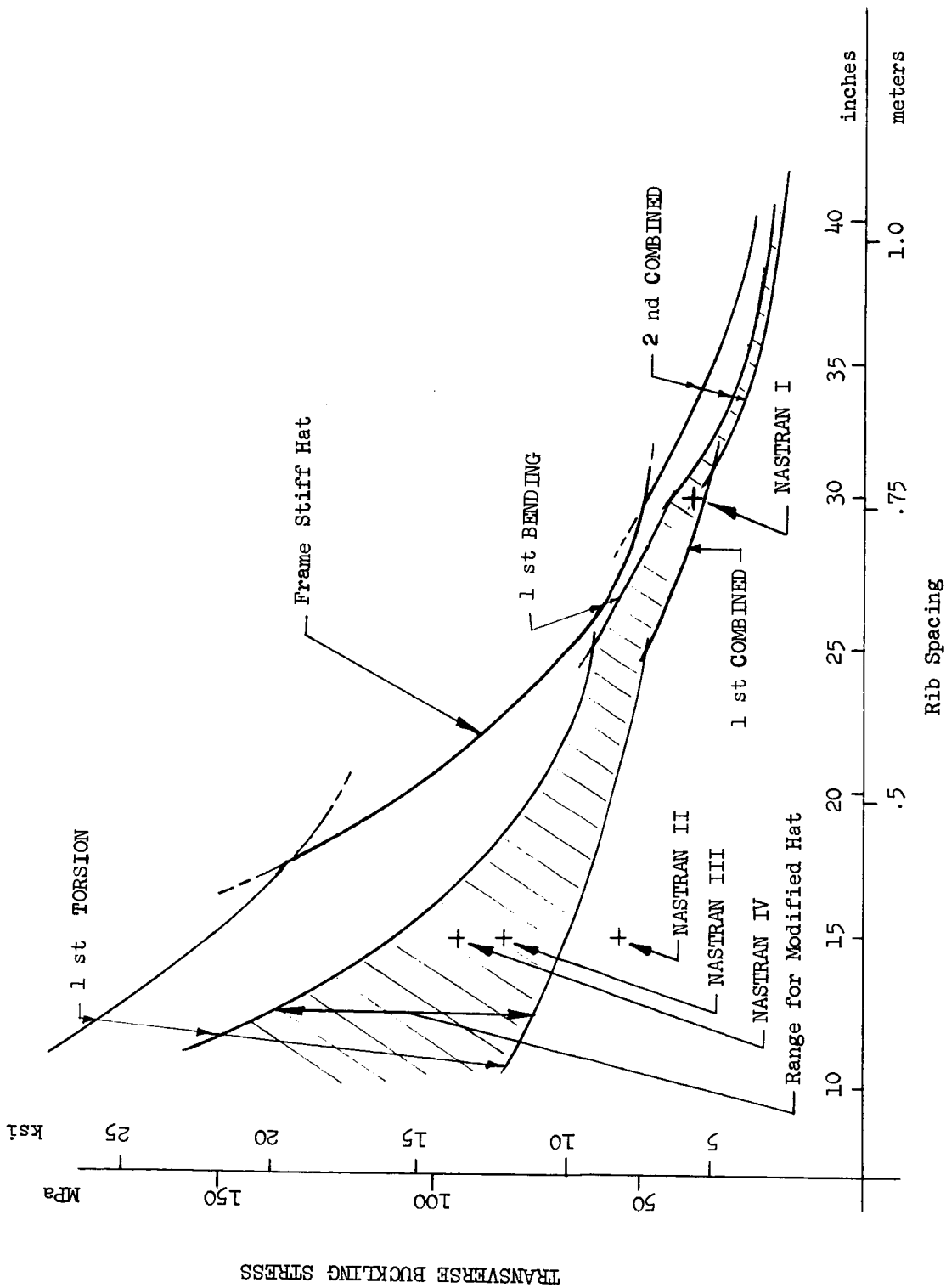


Figure 18.- Effect of design parameters.